Model-independent determination of the strain distribution for a $Si_{0.9}Ge_{0.1}$/Si superlattice using x-ray diffractometry data

A. Yu. Nikulin
School of Physics, University of Melbourne, Parkville, Victoria 3052, Australia

A. W. Stevenson
Commonwealth Scientific and Industrial Research Organization, Division of Materials Science and Technology, Private Bag 33, Clayton South Mail Delivery Center, Victoria 3169, Australia

H. Hashizume*
Research Laboratory of Engineering Materials, Tokyo Institute of Technology, Nagatsuta, Midori, Yokohama 226, Japan
(Received 14 August 1995)

The strain distribution in a $Si_{0.9}Ge_{0.1}$/Si superlattice is determined from x-ray diffractometry data with a 25 Å depth resolution. A logarithmic dispersion relation is used to determine the phase of the structure factor with information available *a priori* on the sample structure. Phase information is obtained from the observed reflection intensity via a logarithmic Hilbert transform and the *a priori* information is used to select the zeros to be included in the solution. The reconstructed lattice strain profile clearly resolves SiGe and Si layers of 90–160 Å thickness alternately stacked on a silicon substrate. The SiGe layer is found to have a lattice spacing in the surface-normal direction significantly smaller than predicted by Vegard's law. The result gives simulated rocking-curve profiles in very good agreement with the observation. The apparent deviation from Vegard's law could be confirmed by chemical analysis.

I. INTRODUCTION

In recent years $Si_{1-x}Ge_x$/Si superlattices on a silicon substrate have received considerable attention because of the prospect of developing silicon-based light-emitting devices for optical communication.[1,2] The indirect nature of the band gap of silicon can be changed by way of zone folding in the SiGe/Si quantum wells. The optical properties of such devices depend upon the microstructures and morphology of thin SiGe layers and their interfaces.[3] X-ray methods have unique advantages over other structure probes in that buried layers and interfaces are investigated nondestructively. The use of intense synchrotron x rays allows atomic resolutions to be obtained in reflectometry and diffractometry measurements. Most studies to date make use of simulations to achieve a fit of measured reflection profiles. Simulations need models and will in general lead to nonunique answers for the density or strain profile. A model-independent method of mapping lattice strains was developed by Petrashen and Chukovskii, which uses a logarithmic dispersion relation to determine the structure-factor phase from a measured x-ray-diffraction profile.[4] The technique has been extended to two-dimensional (2D) distortions in crystals with lateral periodic superstructure modulations.[5] It applies the 1D phase-retrieval formalism to satellite reflections and Fourier synthesizes the solutions to build a 2D strain map. The method was demonstrated in applications to silicon crystals which were ion implanted through periodic surface oxide mask patterns.[5–7]

The present paper describes a model-independent determination of lattice strain in thin SiGe/Si multilayers using the 1D phase-recovery method[4] with nanometer spatial (depth) resolution. Superlattice multilayers involve higher strain gradients in the interface regions than ion-implanted crystals, and the applicability of the technique to such structures has not previously been demonstrated, to our knowledge.

II. EXPERIMENT

Superlattice samples were prepared on symmetric Si(111) wafers using a gas-source molecular-beam-epitaxy facility.[8] A pair of Si(400 Å)/$Si_{0.9}Ge_{0.1}$ (400 Å) bilayers were grown on a homoepitaxial 1-μm-thick Si buffer layer. The indicated alloy composition and layer thicknesses are nominal values to be determined in this study. We carried out x-ray experiments on beamline 20B at the Photon Factory synchrotron source, KEK, Tsukuba, Japan. A double-crystal Si(111) monochromator extracted an x-ray beam of 1.54 Å wavelength from a bending-magnet source, which was incident on the sample oriented for the 111 Bragg reflection. An automatic attenuator inserter was placed after the monochromator to cope with the wide intensity range measured (6 decades). A slit and antiscatter shielding resulted in a beam with dimensions 0.1 mm vertically (in the plane of diffraction) and 2.0 mm horizontally being incident on the sample. The analyzer crystal, which was mounted on the detector arm with a scintillation counter, is a four-reflection symmetric Si(111) monolith. The overall arrangement of these crystal elements is $(+,-,+,-,+,-,+)$. The whole assembly, except the monochromator, was housed in the evacuated drum (1 Torr in pressure) of the "BIGDIFF" diffractometer[9,10] on beamline 20B, whereby air scattering was reduced. To measure a two-dimensional intensity map in the vicinity of the Si 111 Bragg peak, a series of sample (ω) scans were performed for fixed positions of the analyzer/detector (2θ). The nominal step sizes were 0.0003° in ω and 0.007° in 2θ. The parallelogram covered in (ω, 2θ) space (where ω and 2θ are plotted as orthogonal axes) has sides parallel to the ω axis and to the

line given by $2\omega=2\theta$, which represents the direction of the crystal truncation rod (CTR) for a symmetric sample. CTR scattering originates from an abrupt truncation of the periodic charge density at a crystal surface.

Intensity distributions in angular $(\omega, 2\theta)$ space are transformed to reciprocal (q_x, q_z) space by

$$q_x=(2\omega-2\theta)\sin\ \theta_B/\lambda, \tag{1}$$

$$q_x=2\theta\ \cos\ \theta_B/\lambda, \tag{2}$$

where θ_B is the Bragg angle and λ is the x-ray wavelength. $\omega=2\theta=0$ is located at the Bragg peak. The intensity map occupies a rectangular area in reciprocal space, with the CTR direction parallel to q_z. The nominal step sizes correspond to 1.74×10^{-5} and 7.6×10^{-4} nm^{-1} in q_x and q_z, respectively, and the corresponding ranges are 6.87×10^{-4} and 4.10×10^{-1} nm^{-1}.

III. PHASE RETRIEVAL METHOD

In the kinematical approximation, for the case of 1D lattice distortions, the amplitude reflection coefficient for diffracted x rays can be written in the form[4]

$$R(q_z)=\int_0^\infty \psi_h(z)e^{-\mu z}e^{iq_z z}dz, \tag{3}$$

where $\psi_h(z)$ is proportional to the structure factor of the distorted crystal and μ is the x-ray-absorption coefficient. We define the phase $\phi(q_z)$ of $R(q_z)$ by $R(q_z)=|R(q_z)|\exp[i\phi(q_z)]$. For small atomic displacements $u(z)$

$$\psi_h(z)=\psi_h^{\rm perf}\ \exp[2\pi i\mathbf{h}\cdot\mathbf{u}(z)], \tag{4}$$

where $\psi_h^{\rm perf}$ is proportional to the structure factor of a perfect crystal and h is the reciprocal-lattice vector.[11] The phase of $\psi_h(z)$ is thus $\phi_h^{\rm perf}+2\pi\mathbf{h}\cdot\mathbf{u}(z)$ where $\phi_h^{\rm perf}$ is the phase of $\psi_h^{\rm perf}$. Equation (4) is not valid for large $|\mathbf{u}(z)|$, but the change of the phase of $\psi_h(z)$ from $\phi_h^{\rm perf}$ is still given by $2\pi\mathbf{h}\cdot\mathbf{u}(z)$. If the phase $\phi(q_z)$ of $R(q_z)$ is determined from the measured intensity $I(q_z)=|R(q_z)|^2$, the projection of $\mathbf{u}(z)$ onto h can be determined via Eqs. (3) and (4). For this purpose we extend the function $R(q_z)$ into the complex momentum-transfer plane, by changing q_z to complex Q_z. $R(q_z)$ is the value of $R(Q_z)$ on the real axis of the complex Q_z plane. $R(Q_z)$ is analytic for $\mathrm{Im}Q_z>-\mu$ since $|\psi_h(z)|$ is finite. It is more convenient to treat the function[4]

$$\tilde{R}(q_z)=-i(q_z+i\mu)R(q_z)=\psi_h(0)+\int_0^\infty \psi_h'(z)e^{-\mu z}e^{iq_x z}dz \tag{5}$$

representing the normalized amplitude, since this function, when continued into the complex Q_z plane, is analytic at all Q_z because $\psi_h'(z)=0$ for $z\geqslant T$, where T is the thickness of the distorted surface layer lying on a perfect-crystal substrate. As shown by Petrashen and Chukovskii,[4] if the following condition is valid:

$$\int_0^\infty |\psi_h'(z)|e^{-\mu z}dz<|\psi_h(0)|, \tag{6}$$

the function $\tilde{R}(Q_z)=|\tilde{R}(Q_z)|\exp[i\tilde{\phi}(Q_z)]$ is not zero for $\mathrm{Im}Q_z>0$ or has no zero in the upper half Q_z plane (uhp). In this case the real and imaginary parts of $\ln\tilde{R}(q_z)$ are related by the logarithmic Hilbert transform:[12]

$$\tilde{\phi}(q_z)=-\frac{1}{\pi}\mathscr{P}\int_{-\infty}^{\infty}\frac{\ln|\tilde{R}(q_z')|}{q_z'-q_z}\,dq_z', \tag{7}$$

where $\mathscr{P}$ denotes the Cauchy principal value. A slightly different form of the logarithmic dispersion relation has been derived from Titchmarsh's theorem for the causal transform and quoted for phase determination in reflectivity measurements involving x rays and neutrons.[13,14] If the reflection amplitude has no complex zeros in the uhp, the phase of the structure factor is completely determined by the measured intensity. The resultant solution is denoted the minimal-phase solution in our previous papers.[6,7] The phase $\tilde{\phi}(q_z)$ is related to the phase required, $\phi(q_z)$, via Eq. (5). Observed diffraction intensities $I(q_z)=|R(q_z)|^2$ are corrected for the $1/q_z^2$ decay and absorption (μ) to give a normalized intensity profile $\tilde{I}(q_z)$, which is fit with a polynomial function. This function corresponds to

$$\tilde{I}(Q_z)=\tilde{R}(Q_z)\tilde{R}^*(Q_z^*), \tag{8}$$

in the complex plane, where $*$ indicates a complex conjugate.[4] This expression of intensity is adopted instead of $\tilde{I}(Q_z)=\tilde{R}(Q_z)\tilde{R}^*(Q_z)$ because it is analytic in the complex plane while the latter is not. For real Q_z the two expressions give $\tilde{I}(q_z)=|\tilde{R}(q_z)|^2$. If $\tilde{I}(Q_z)=0$, or has zeros, at Q_{zj} $(j=1,2,\ldots,M)$ in the uhp, the phase of $\tilde{R}(Q_z)$ on the real axis is given by

$$\tilde{\phi}(q_z)=\tilde{\phi}_H(q_z)+\sum_j\ \arg\frac{q_z-Q_{zj}}{q_z-Q_{zj}^*}, \tag{9}$$

where $\tilde{\phi}_H$ is the Hilbert (or minimal) phase given by Eq. (7). The term $(q_z-Q_{zj}^*)$ appears in Eq. (9) because replacing Q_{zj} by Q_{zj}^* does not affect the modulus of $\tilde{I}(Q_z)$ on the real axis, $\tilde{I}(q_z)$. As is evident from Eq. (8), if $\tilde{I}(Q_{zj})=0$, then $\tilde{I}(Q_{zj}^*)=0$. Hence if $\tilde{I}(Q_z)$ has M zeros in the uhp, it has the same number of zeros in the lhp. Zeros in $\tilde{I}(Q_z)$ occur in pairs (Q_{zj}, Q_{zj}^*). We cannot distinguish the zeros of $\tilde{R}(Q_z)$ from those of $\tilde{R}^*(Q_z^*)$. Taking an arbitrary number of zeros from the uhp, and the rest from the lhp, generates 2^M sets of M phases, giving 2^M possible solutions for $\tilde{R}(Q_z)$. These represent ambiguous solutions in the inverse scattering problem. The function $\tilde{R}(Q_z)$, having M zeros in the uhp, can be expressed as[12]

$$\tilde{R}(Q_z)=\prod_{j=1}^{M}\left(\frac{Q_z-Q_{zj}}{Q_z-Q_{zj}^*}\right)\tilde{R}_H(Q_z), \tag{10}$$

where

$$\tilde{R}_H(q_z)=|\tilde{I}(q_z)|^{1/2}e^{i\tilde{\phi}_H(q_z)}. \tag{11}$$

The first function in the right side of Eq. (10), called the Blaschke product, has a modulus of 1. It is thus clear in Eq. (10) that all 2^M solutions give the same $\tilde{R}(Q_z)$ on the real axis, hence the same theoretical reflection profile $\tilde{I}(q_z)$. To choose the most plausible one we must resort to *a priori*

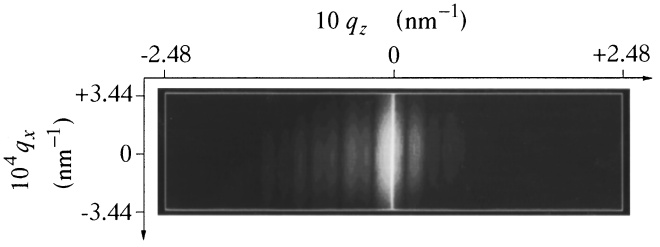

FIG. 1. Scattering intensity distribution in reciprocal space from the Si/SiGe superlattice. The 111 Bragg spot, located at $q_x=q_z=0$, has full widths at half maxima of 1.3×10^{-4} and 7.3×10^{-4} nm^{-1} in q_x and q_z, respectively, the apparent elongation only being a result of the scales used for q_x and q_z.

information about the sample structure under investigation. Incidentally, $\arg[(q_z-Q_{zj})/(q_z-Q_{zj}^*)]$ is equivalent to $2\arg(q_z-Q_{zj})$ in Eq. (9). If $\tilde{I}(Q_z)=0$ at Q_{zj} in the uhp, $\tilde{\phi}(q_z)$ thus increases by 2π when q_z is scanned from $-\infty$ to $+\infty$. A plot of $\tilde{\phi}(q_z)$ will show an appreciable change near $q_{zj}=\mathrm{Re}Q_{zj}$.

A practical procedure calculates the minimal-phase solution for $\tilde{R}(Q_z)$ using a polynomial function of power M for $\tilde{I}(Q_z)$ and finds the Hilbert phase $\tilde{\phi}_H(q_z)$. The minimal-phase solution has all zeros in the lhp. The polynomial interpolation produces M zeros of $\tilde{I}(Q_z)$, which are flipped about the real axis to generate M zeros in each of the uhp and the lhp. Phase $\phi(q_z)$, derived from $\tilde{\phi}_H(q_z)$ via the first part of Eq. (5), is used to obtain $R(q_z)=I(q_z)^{1/2}\exp[i\phi(q_z)]$. An inverse Fourier transform of $R(q_z)$ gives $\psi_h(z)\exp(-\mu z)$, which is used to find $\mathbf{h}\cdot\mathbf{u}(z)$ by Eq. (4). If this $\mathbf{h}\cdot\mathbf{u}(z)$ is inconsistent with the *a priori* sample information, one of the M zeros in the uhp is added to the minimal-phase solution to produce a new solution. This procedure is repeated until we arrive at a plausible solution. The power M of the fitting polynomial function is decided primarily by consideration of the thickness of the surface layer to be investigated and the desired depth resolution. The angular range of the data used in the analysis determines a maximal depth resolution of the resultant strain profile:

$$\Delta z=\frac{1}{q_z^{\max}}=\frac{\lambda}{(2\theta)^{\max}\cos\theta_B}. \tag{12}$$

This indicates 25 Å for our experiment.

IV. RESULTS

Figure 1 shows the triple-crystal intensity data plotted in 2D reciprocal space, after normalization according to the flux-monitor readings. The 111 Bragg spot, located at $q_x=q_z=0$, looks like a line extended in the q_x direction. This is due to the largely expanded q_x scale. No truncation rod is apparent in the q_z direction. The small q_x range covered makes it hard to see a well defined CTR. To reconstruct the lattice strain profile we only used the intensity distribution along q_z with $q_x=0$ and discarded other data. One may suppose that such data could be collected by a simple 1D $\omega-2\theta$ scan, rather than time-consuming 2D scans. 1D scans will not work, however, because the mechanical accuracy of the x-ray diffractometer is insufficient to keep track of the CTR peak. The data was processed with numerical programs

TABLE I. Results of a least-squares fit of the x-ray reflectivity data. Gaussian root-mean-square roughness refers to the top interface of the relevant layer. Numbers in parentheses show standard deviations.

Layers	Layer thickness (Å)	RMS roughness (Å)
Si	137.03(2.8)	9.29(2.8)
$Si_{0.9}Ge_{0.1}$	146.24(3.3)	9.36(3.1)
Si	164.4(3.4)	12.69(6.6)
$Si_{0.9}Ge_{0.1}$	93.97(3.7)	17.59(15.0)

using the formalism described in Sec. III, which gave a complex function $\psi_h(z)$. Extracting the phase of this function, we found displacement $u_z(z)$ and its derivative du_z/dz. A preliminary analysis of the intensity data suggested that the total thickness of the actual superlattice layer is close to 550 Å, but not to the design value of 1600 Å.

To check the thickness of the Si and SiGe layers we collected x-ray reflectivity data. A fit of the specular reflectivity profile yielded the parameter values listed in Table I. The result shows that the Si and SiGe layers have a thickness of 90–160 Å each, instead of 400 Å (the design value). The discrepant thickness is believed to be evidence of distinct crystal-growth processes on the Si(100) and Si(111) substrates, by molecular-beam epitaxy. The crystal grower applied experience on the (100) substrate to the preparation of our (111) sample.

Vegard's law indicates a 0.4% expanded bulk $Si_{0.9}Ge_{0.1}$ lattice relative to bulk silicon. This information, combined with the layer thicknesses in Table I, provides the steplike model strain profile shown in Fig. 2 (broken line). The solid lines plot the strains $\Delta d(z)/d$ determined from the x-ray data, where d is the bulk Si(111) lattice spacing. These solutions rely on the *a priori* information that the strain profile has a two-bilayer structure and that the SiGe layers have larger lattice spacings than the Si layers. The analysis was

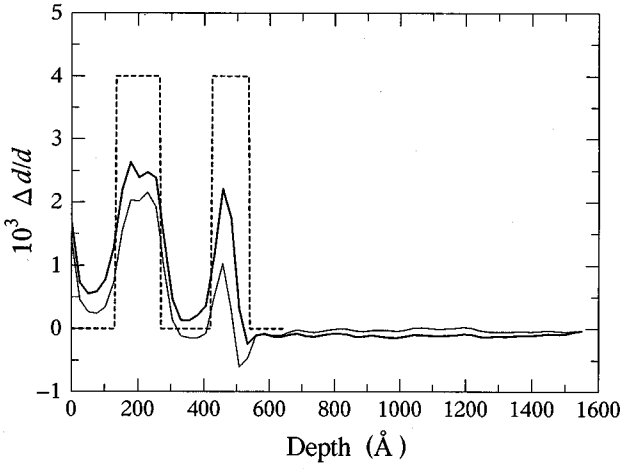

FIG. 2. Strain profiles for the Si/SiGe superlattice derived from the minimal-phase solution (thin solid line) and a solution including one zero (thick solid line). The ordinate represents the relative variations of the (111) lattice spacing from that of bulk silicon. The broken line shows the steplike model strain profile with the layer thicknesses determined by a fit of the specular reflectivity data. The peaks correspond to the SiGe layers and the valleys to the Si layers.

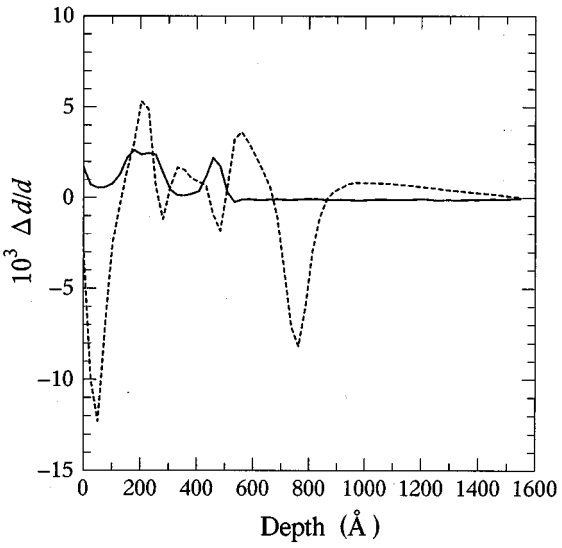

FIG. 3. Strain profiles obtained from a solution including one zero (solid line) and a solution including three zeros (broken line) for the Si/SiGe superlattice.

made for the top 1600 Å layer of the sample with the maximal depth resolution of 25 Å. The minimal-phase solution unravels the two-bilayer structure with the thickness of each layer consistent with the model (Fig. 2, thin solid line). The valley-peak profile exhibits the alternating Si and SiGe layers from top to bottom. The strain-free silicon buffer is also well reproduced in the top 1000 Å. It shows, however, a negative peak at the interface to the buffer layer. The solution

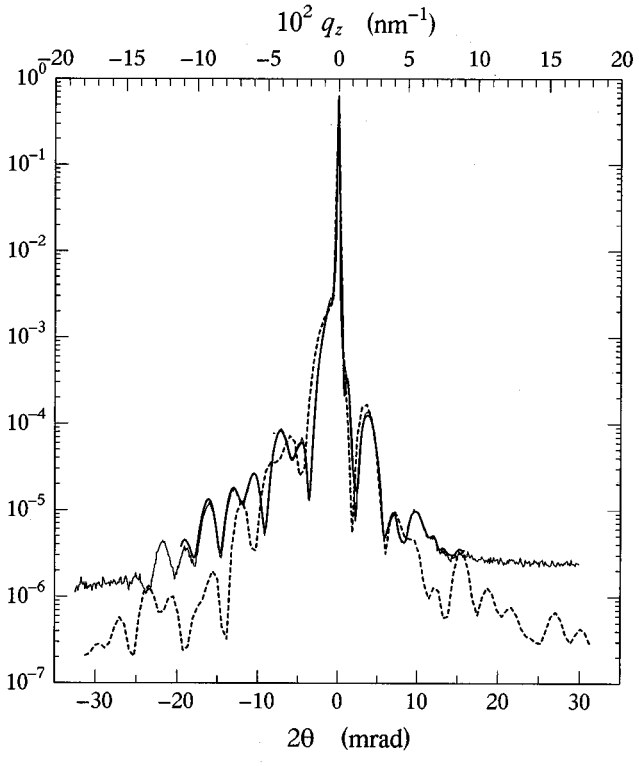

FIG. 4. Experimental (thin line) and calculated (thick line) rocking curves for the one-zero solution. The broken curve is calculated for the steplike model strain profile (broken line in Fig. 2).

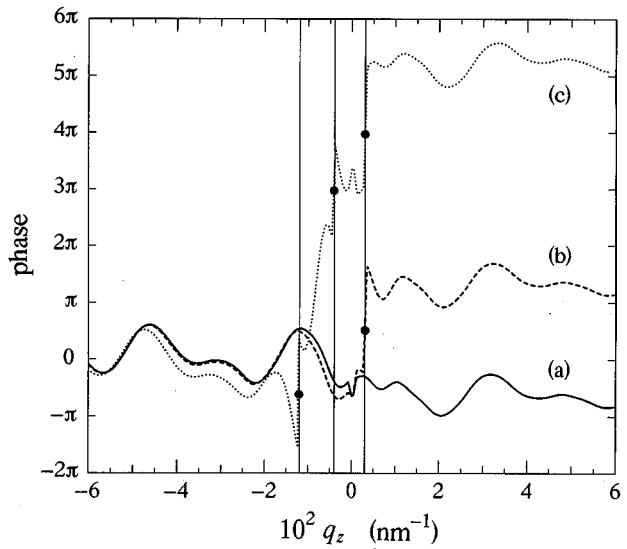

FIG. 5. Structure-factor phases. (a) Hilbert phase $\tilde{\phi}_H(q_z)$, (b) phase $\tilde{\phi}(q_z)$ of the solution including a zero at $(0.003+0.15i)$ nm^{-1}, (c) $\tilde{\phi}(q_z)$ with inclusion of two more zeros at $(-0.0046+0.35i)$ and $(-0.012+0.78i)$ nm^{-1}. Filled circles indicate 2π phase shifts occurring at the zeros.

obtained by adding a zero at (0.003 +0.15i) nm^{-1} to the minimal-phase solution has no negative peak and shows a very similar profile (Fig. 2, thick solid line). We call this solution the one-zero solution hereafter. Solutions including extra zeros are inconsistent with the *a priori* sample information. One example is shown in Fig. 3, where the broken profile was derived from a solution including two more zeros at $(-0.0046+0.35i)$ and $(-0.012+0.78i)$ nm^{-1}. We did not examine all 2^{64} solutions, but our experience shows that we only have to consider zeros close to the Bragg point, $Q_z=0$.

The two peaks in the ''one-zero'' strain profile have heights 2.3–2.6$\times10^{-3}$ (Fig. 2), which are one half the prediction by Vegard's law assuming a $Si_{0.9}Ge_{0.1}$ composition. The actual Ge composition could be checked by secondary ion mass spectrometry or Rutherford backscattering. The profile also shows considerably graded Si/SiGe interfaces. To check the obtained solution we back calculated the rocking curves from the strain profile, using the Takagi formula.[11] In Fig. 4 the simulated curve is barely distinguishable from the experimental one, showing a remarkable agreement. There is a much better fit to the observation than is the case for the curve calculated for the steplike model strain profile (see broken line in Fig. 4).

V. DISCUSSION

When the reflectance has complex zeros, the phase determination via the logarithmic dispersion relation is plagued with the nonuniqueness problem. The physical meaning of a complex zero is that the phase of the x-ray wave changes its value through 2π. This is illustrated in Fig. 5 which plots the phases $\tilde{\phi}(q_z)$ of the minimal-phase, one-zero, and three-zero solutions for our superlattice sample. There is no general solution to this ''phase problem,'' but it is possible to reduce the phase ambiguity using the available information. In the case of our superlattice sample the polynomial interpolation

of $\tilde{I}(Q_z)$ produced 64 complex zeros. The number of physically significant zeros can be known from approximate information about the thickness of distorted layers and the strain amplitudes.

For the phase of an x-ray wave to be shifted by 2π on Bragg reflection at a crystal surface, the surface lattice plane must be displaced by more than one interplanar spacing d by the strain field in the crystal. For this lattice-plane displacement prior information allows us to estimate the number of zeros to be included in the solution. The displacement of the surface plane is given by

$$u_{\mathrm{surf}}=\int_0^T \frac{\Delta d(z)}{d}\, dz. \tag{13}$$

Assuming the lattice constant derived from Vegard's law ($\Delta d/d=4\times10^{-3}$) and the total thickness 250 Å for the two $Si_{0.9}Ge_{0.1}$ layers, we find $u_{\mathrm{surf}}=1$ Å for our SiGe/Si superlattice. The spacing of the Si(111) lattice planes is 3.135 Å. We thus know that the most plausible solution includes no or one zero. Experiences show that for the latter case the zero located near $Q_z=0$ is to be included. The two solutions in Fig. 2 actually exhibit very similar strain profiles. The one-zero solution appears to be more reasonable with no negative peak at the buffer interface.

Both the minimal-phase and one-zero solutions indicate appreciable strain at the surface of the superlattice in Fig. 2. The top silicon surface is likely to be covered by an oxide layer, although we have no evidence. A simulation assuming a suppressed surface strain peak yielded a rocking curve in disagreement with the observation, suggesting that the lattice spacing is actually expanded in the surface region. The strain profile determined can be distorted by the data cutoff. The distortion will be marginal, however, as evidenced by the very good agreement of the simulated rocking curve with the experimental one (Fig. 4). This convinces us that the thin Si and SiGe layers are actually strained as revealed in Fig. 2. The ''one-zero'' strain profile shows that relative to the steplike model, the Si lattice is expanded by 0.02–0.06 %, while the SiGe lattice is contracted by 0.15–0.2 % in the surface normal direction. A simple picture of epitaxial Si and SiGe lattices can hardly explain these strains. The quite large negative strain (relative to the steplike model) found for the SiGe layers suggests a smaller Ge composition than the nominal value ($x=0.1$).

For the determination of strain profiles simulations are commonly used to fit the measured reflection profile.[15–17] Simulations need a model and will in general lead to nonunique answers for the strain profile (see below). As stated in Sec. III, there are in general a large number of strain profiles giving exactly the same reflection profile. All these strain profiles can have very different shapes. A lucid account is given by Reiss and Lipperheide[18] for the case of the density profiles (scattering potentials) in neutron reflectometry. In our case, all the three strain profiles shown in Figs. 2 and 3, as well as all the other solutions, produce the same rocking curve shown in Fig. 4 (thick solid line). They are derived from solutions including different numbers of zeros and constitute a family of ''reflection-equivalent'' strain profiles.[18] A real problem with the inversion procedure is that one cannot examine a large number of solutions including zeros. In this connection, the importance of various theoretical and experimental attempts to reduce the phase ambiguity cannot be overemphasized.

Simulations require a good starting model. In the case of our multilayer sample, a model assuming the design layer thickness, 400 Å for each Si and SiGe layer, could lead a simulation to an incorrect result or a least-squares fit could fail to reproduce the observed reflection profile. The approach using the logarithmic dispersion relation to solve the inverse scattering problem requires more complicated formalisms and numerical programs, and can result in ambiguous answers, but depends on no model. Approximate *a priori* information on the sample structure helps in arriving at a correct solution, at least for certain profiles, as demonstrated in this work.

The technique can be applied to more complicated multilayer structures than studied here. A limiting factor is the maximal number of zeros that we can handle. This determines the total thickness of the reconstructed layer and the depth resolution, since in our algorithm the number of zeros is equivalent to the number of depth resolution elements used in the analysis. Our current software and computer capacity allows us to treat 128 zeros, and so a superlattice with ten pairs of 50-Å-thick SiGe/Si bilayers can be investigated with 5 Å resolution, unless the top-layer lattice plane is shifted by many multiples of the d spacing. A high-resolution analysis requires data to be collected far from the Bragg peak [see Eq. (12)], but a 3–5 Å depth resolution will be achieved on a low-background synchrotron beamline. Possible overlaps of neighboring CTR scatterings can be avoided with slightly miscut samples. A more complete discussion about the application limit of our technique will appear in a forthcoming paper.

ACKNOWLEDGMENTS

We thank Y. Shiraki for the sample provision. Contributions from Y. Yamaguchi, and T. Ohkawa in the specular reflectivity measurement are appreciated. We also appreciate discussion with P. Petrashen, K. Nugent, and T. Gureyev. The computer code used in this work was originally developed by P. Petrashen and we thank him for making it available to us. The synchrotron experiment described in this work was supported by the Photon Factory under proposal 94G347 and the Australian National Beamline Facility (ANBF). A.Y.N. acknowledges the support from an ARC Grant. This work is supported by Monbusho International Scientific Research Program, No. 04044066, and Grant-in Aid for Scientific Research, No. 06452310.

*Author to whom all correspondence should be addressed.

[1] H. Presting, H. Kibbel, M. Jaros, R. M. Turton, U. Menzigar, G. Abstreiter, and H. G. Grimmeiss, Semicond. Sci. Technol. **7**, 1127 (1992).

[2] P. Zaumseil, U. Jagdhold, and D. Kruger, J. Appl. Phys. **76**, 2191 (1994).

[3] H. Sunamura, Y. Shiraki, and S. Fukatsu, Appl. Phys. Lett. **66**, 953 (1995).

[4] P. V. Petrashen and F. N. Chukhovskii, Sov. Phys. Dokl. **34**, 957 (1989).
[5] T. E. Goureev, A. Yu. Nikulin, and P. V. Petrashen, Phys. Status Solidi A **130**, 263 (1992).
[6] A. Yu. Nikulin, O. Sakata, H. Hashizume, and P. V. Petrashen, J. Appl. Crystallogr. **27**, 338 (1994).
[7] A. Yu. Nikulin *et al.*, J. Appl. Crystallogr. **28**, 803 (1995).
[8] S. Fukatsu *et al.*, Appl. Phys. Lett. **61**, 804 (1992).
[9] Z. Barnea *et al.*, Rev. Sci. Instrum. **63**, 1069 (1992).
[10] A. Yu. Nikulin *et al.*, J. Appl. Crystallogr. **28**, 57 (1995).
[11] S. Takagi, J. Phys. Soc. Jpn. **26**, 1239 (1969).
[12] R. E. Burge, M. A. Fiddy, A. H. Greenway, and G. Ross, Proc. R. Soc. (London) **350**, 191 (1976).
[13] W. L. Clinton, Phys. Rev. B **48**, 1 (1993).
[14] R. Lipperheide *et al.*, Phys. Rev. B **51**, 11 032 (1995).
[15] J. G. E. Klappe and P. F. Fewster, J. Appl. Crystallogr. **27**, 103 (1994).
[16] M. Servidori and R. Fabbri, J. Phys. D **26**, A22 (1993).
[17] A. A. Stepanov, J. Appl. Phys. **27**, 7 (1994).
[18] G. Reiss and R. Lipperheide, Physica B (to be published).